Radar Range Deception With Time-Modulated Scatterers

Vitali Kozlov, Dmytro Vovchuk, and Pavel Ginzburg, *Member, IEEE*

***Abstract*— Modern radar systems are designed to have high Doppler tolerance to detect fast-moving targets. This means range and Doppler estimations are inevitably coupled, opening pathways to concealing objects by imprinting artificial Doppler signatures on the reflected echoes. Proper temporal control of the backscattered phase can cause the investigating radar to estimate the wrong range and velocity, thus cloaking the real position and trajectory of the scatterer. This deception method is exploited here theoretically for arbitrary Doppler tolerant waveforms and then tested experimentally on an example of the linear frequency modulated (LFM) radar, which is the most common waveform of that class used in practice. The method allows retaining radio silence with a semi-passive (battery-assisted) approach that can work well with time-dependent metasurfaces. Furthermore, as an insight into new capabilities, we demonstrate that temporally concealed objects could even be made to appear closer than they truly are without violating the laws of relativity.**

***Index Terms*— Electronic counter-countermeasures (ECCMs), electronic countermeasures (ECMs), radar deception.**

I. Introduction

CONTEMPORARY radar systems play a significant role in numerous sensing applications [1], [2], [3], [4], [5], [6], [7] and are likely to remain just as relevant in the foreseeable future, both as standalone platforms as well as parts of a fused sensory network. The key advantage of such systems lies in their relatively low operational frequency band in the electromagnetic spectrum, allowing interrogation through fog and other obstacles that render optical investigation difficult. The vital importance of such systems, as well as their analogs in sonar and light detection and ranging (LIDAR), birthed entire scientific and technological branches, ushering advances in both hardware and software solutions [8], [9], [10], [11], [12]. The success and proliferation of radar systems were inevitably met with a relentless pursuit for electronic countermeasures (ECMs) to avoid detection, which was themselves soon followed by electronic counter-countermeasures (ECCMs) and so on [13], [14], [15], [16], [17], [18]. Stealth technologies were introduced to minimize the signatures measured by the receivers [19], [20], offering a passive solution to the problem of evading detection without transmitting electromagnetic radiation, which could expose the radar to honing by a sophisticated ECCM system. Yet no matter how absorbent the material is, no matter how careful the geometry is designed, the detectability range could only be reduced by a finite factor which could be overcome by a radar transmitting more power. Moreover, multi-static radars and interrogation by discerning reflection from upper layers of the atmosphere can challenge stealth technologies quite significantly. To further confuse the investigating radar, jamming measures were soon added.

By actively transmitting noise toward the radar, its dynamic range could be reduced, and detection probability diminished at the cost of foregoing radio silence. Spoofing methods followed, with the most rudimentary solutions being the release of chaff to decoy the radar [21], [22], [23], [24], and the more advanced was the introduction of repeaters that could imprint careful signatures on the reflected echoes, causing the radar to deduce the wrong trajectory and location of the targets of interest, producing so-called ghosts [25], [26], [27], [28]. The drawback of such methods was rooted in their failure to suppress the echo from the target itself, relying instead on amplifying the spoofed echoes from the repeater, in an attempt to draw the radar to track the larger return rather than the object of interest. It did not take long for spoofing ECM to be met with smart ECCM signal processing [29], [30], [31], severely challenging its effectiveness. In recent years, the emerging field of metamaterials and metasurfaces had rapidly developed [32], [33], [34], enabling novel types of passive stealth capabilities not possible before [35], [36], [37].

Today, dynamic control over metamaterial scattering properties is a rapidly developing field. By carefully controlling the reflection coefficient of the scatterer in time, it is possible to imprint arbitrary signatures on the backscattered echoes [38], [39], [40], [41], [42] as well as modulate it in a way that would spread the spectrum over a large bandwidth [43], [44]. The goal of such meta-covers is to achieve the advantages of state-of-the-art repeaters without suffering from the drawback of merely superimposing on top of the reflection from the real target. The concept of using metamaterial surface covers is illustrated in Fig. 1, where a drone (as an illustrative example) is depicted with and without a time-dependent cloak while it is observed by the same radar system. The concealed drone in Fig. 1(b) successfully modulates the reflected echoes in such a way that it appears closer than it really is. This statement might at first appear to contradict intuition, seeing as a pulse cannot travel faster than light. This apparent "faster than light travel" can only

Manuscript received 27 November 2022; revised 21 January 2023; accepted 10 February 2023. Date of publication 14 March 2023; date of current version 5 May 2023. This work was supported in part by the Department of the Navy, Office of Naval Research Global (ONRG), under Award N62909–21–1–2038. *(Corresponding author: Vitali Kozlov.)*

The authors are with the Department of Physical Electronics, Tel-Aviv University, Tel Aviv 69978, Israel (e-mail: vitaliko@mail.tau.ac.il).

Color versions of one or more figures in this article are available at https://doi.org/10.1109/TAP.2023.3255108.

Digital Object Identifier 10.1109/TAP.2023.3255108

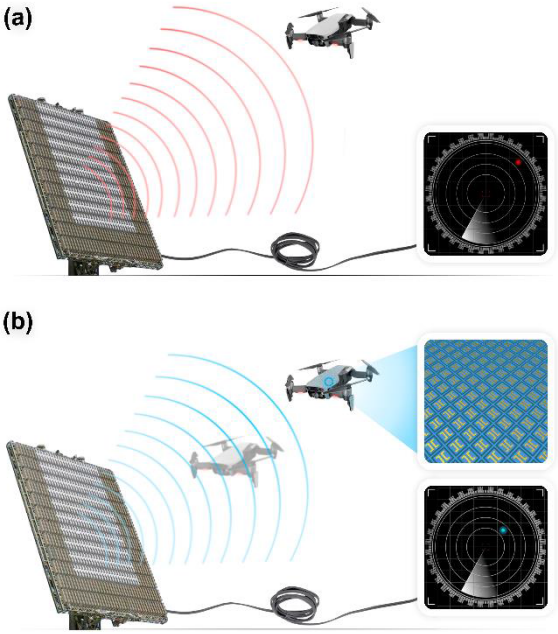

Fig. 1. Illustration of the proposed deception application. A radar observing a drone with and without time-dependent metasurface cover. (a) Drone without cover is correctly detected. (b) Dynamic control of the scattering properties from the drone conceals its true location, making it appear closer (or further, on demand) than it really is with respect to the investigating radar. Note that a single scatterer is demonstrated in the manuscript.

be achieved for a certain, yet widely used class of radar signals, as will be discussed ahead. Note, that hereinafter, we will investigate the performances of a single scatterer rather than a metasurface. The manuscript is organized in the following way. Section II is a theoretical derivation of the proposed deception concept. Section III discusses ECCMs. Here, a general class of Doppler-tolerant waveforms is presented. Section IV is an experiment, conducted in the anechoic chamber, showing that it is indeed possible to manipulate a frequency-modulated continuous waveform (FMCW) radar to conclude the arbitrary position of the scatterer with dynamic control over the scattered phase. Section V is an outlook and conclusions.

II. Theory-Range Deception of Doppler Tolerant Radars

Radar systems rely on signal processing to extract information about the observed environment from reflected echoes. To achieve this, the transmitted waveform needs to be carefully selected to meet specifications. The parameters of interest are, among others, range and Doppler resolutions [45], [46], [47], which are preferably as high as possible. These metrics of a waveform $s(t)$ can be conveniently viewed through the narrowband ambiguity function (wideband signals are beyond the scope of this manuscript), given by Levanon and Mozeson [45]

$$\chi_{S(t)}(\tau,\omega_D)=\int_{-\infty}^{\infty}e^{-i\omega_D t}s(t)s^*(t-\tau)dt. \tag{1}$$

This is a function of the Doppler frequency ω_D due to the motion of the reflecting point-like target, located at a distance R, which translates to delay $\tau=(2R/c)$ through the speed of light c. The function in (1) describes the output of the matched filter for a specific waveform, which ensures a maximal signal-to-noise ratio at the range of the target. In other words, the matched filter is searching for the signal in the sampled data by correlating it with the known transmitted waveform, while the ambiguity function also considers the output due to possible distortion of the returning echo by the Doppler effect. Consider three commonly used waveforms with compact support on $(0,T)$ [45]

$$s_{\text{Noise}}(t)=n_\sigma(t)u\left(\frac{t}{T}\right) \tag{2}$$

$$s_{\text{LFM}}(t)=e^{-i\left(\omega_0+\frac{\Delta_\omega}{2T}t\right)t}u\left(\frac{t}{T}\right) \tag{3}$$

$$s_{P_3}(t)=e^{-i\varphi_M(t)}u\left(\frac{t}{T}\right) \tag{4}$$

where T is the duration of the signal, $u(t)=\begin{cases}1 & 0<t<1\\ 0 & o.w\end{cases}$ is the rectangular pulse function, $n_\sigma(t)$ is a zero-mean complex Gaussian random process with standard deviation σ, ω_0 is the initial frequency of the linear frequency modulated (LFM) chirp, which can be positive (up chirp) or negative (down chirp), and Δ_ω is the bandwidth of the chirp, i.e., the maximal deviation from the initial frequency. The polyphase waveform P_3 in (4) can be thought of as an M-sampled variation of the LFM, with the phases $\varphi_M(t)=\sum_{m=1}^{M}\varphi_m u((t-(T/M)(m-1)/(T/M)))$ and $\varphi_m=(\pi/M)(m-1)^2$. This is the place to note that the complex analytical representation of the signals is used throughout the manuscript.

Fig. 2 shows the ambiguity function of the above waveforms for arbitrarily selected parameters, where the signal duration is $T=50$ μs, the sample rate is 5 MHz and the pulse repetition frequency (PRF) is 10 kHz. The axes are normalized to present fractional Doppler to bandwidth ratio $((\omega_D/\Delta_\omega))$ and range to unambiguous range ratio $((R/R_{\text{unambiguous}}))$ for illustrative purposes, as will be discussed ahead. Note that positive Doppler frequencies represent approaching targets while negative Doppler frequencies represent receding targets.

Fig. 2(a) shows the results for the noise waveform in (2) with $\sigma=1$, having a very well-defined peak at the origin, often called a "thumbtack," which achieves excellent range and Doppler resolutions (recall that the cross-correlation of white noise is a delta function, which is appealing for obtaining superior range resolution). However, the noise waveform suffers immensely from Doppler intolerance, which means that if the reflecting target was moving, the output of the matched filter would be a horizontal cut above or below the origin, where no ambiguity volume is left, rendering the target practically invisible. To overcome this issue, it is better to have a "ridge-like" autocorrelation function, such as illustrated in Fig. 2(b) and (d), showing the ambiguity function of the LFM waveform in (3) within an up and down chirp respectively of $|\Delta_\omega|=2\pi\times 0.5$ MHz and $\omega_0=0$ for simplicity. This is the most commonly used Doppler tolerant waveform at the present day and it will be used for the experiment ahead. This waveform clearly has a significant output even for a

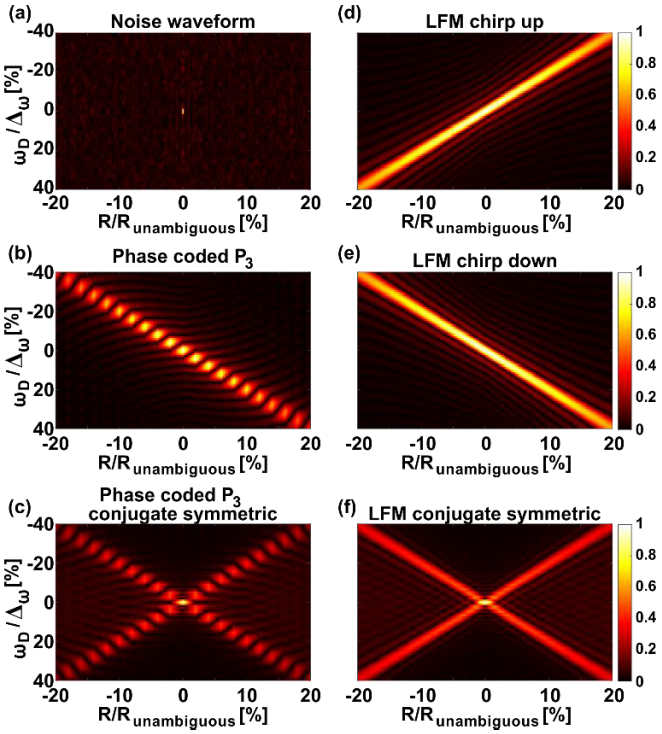

Fig. 2. Absolute values of the ambiguity function of six different waveforms as a function of fractional Doppler to bandwidth ratio and range to unambiguous range ratio. (a) Noise waveform. (b) Phase coded P_3. (c) Phase coded P_3 after CS appending. (d) LFM chirp up. (e) LFM chirp down. (f) LFM after CS appending (chirp up then back down).

moving target, as can be seen by taking horizontal cuts of the plots. While the term "Doppler tolerance" is somewhat open to interpretation [48], [49], [50], it can be said that any waveform that can still produce a strong output for a significant band of Doppler frequencies is tolerant. Another example of such a waveform appears in Fig. 2(c), where the phase coded P_3 waveform in (4) with $M = 25$ is shown. It bears a lot of resemblance to the down-chirped LFM, but with visible gaps, meaning that for certain target velocities detection might not be possible. Another apparent result, which can be deduced from the symmetries of the ambiguity function, is that Doppler tolerant waveforms inevitably couple range with Doppler. This means that any moving target would produce an error in the range which in these examples is proportional to the radial velocity of the observed scatterer [51], [52]. This relationship can be exploited by artificially imprinting Doppler signatures on the echoes reflected from the target, as will be shown experimentally ahead. Notice that it is possible to deceive the radar into concluding that the target is even closer than it truly is without violation of relativity, but simply by the virtue of the properties of the matched filter detection method for this class of waveforms. The axes of Fig. 2 are stressing the fact that it is possible to create a significant error in range (positive or negative, at will), reaching as high as 20% from the maximal unambiguous range ($R_{\text{unambiguous}} = (c/2\text{PRF})$), given the parameters set above. It is also evident that such artificial modulation would not lead to the signal being completely filtered out by the bandpass filter of the receiver, since it is well within the required operational bandwidth of the system. By reducing the PRF and increasing the bandwidth of the chirp Δ_ω, the attainable range shift will diminish, and the proposed deception method will be more limited.

III. Countermeasures-CS Waveforms

To counter spoofing attempts of this kind, diversity can be introduced to the transmitted waveform. For example, it is possible to alternate between an up chirp and a down chirp of the LFM, producing two different alternating ranges for the target that can be resolved as the mean of the two. Chirp rate variations can be also employed. Another approach, which to the best of our knowledge is first suggested here, is applicable to all waveforms. By appending any signal $s(t)$ with compact support on $(0, T)$ to its time-reversed and conjugated self, we arrive at the new conjugate symmetric (CS) waveform

$$s_{\text{CS}}(t) = s(t) + s^*(-t + 2T) \tag{5}$$

which is of length $T_{\text{CS}} = 2T$ and has the symmetric property around its center $s_{\text{CS}}((T_{\text{CS}}/2) - t) = s^*_{\text{CS}}((T_{\text{CS}}/2) + t)$. It is straightforward to show by substitution to (1) that the ambiguity function of these special waveforms is symmetric with respect to both axis

$$\begin{aligned}|\chi_{S_{\text{CS}}(t)}(\tau, \omega)| = |\chi_{S_{\text{CS}}(t)}(-\tau, \omega)| = |\chi_{S_{\text{CS}}(t)}(\tau, -\omega)\\ | = |\chi_{S_{\text{CS}}(t)}(-\tau, -\omega)|.\end{aligned} \tag{6}$$

The result of applying the CS process to the P_3 and LFM waveforms is shown in Fig. 2(c) and (f) respectively, where the symmetry of the ambiguity function is apparent. Such waveforms would produce two separate peaks in the autocorrelation (horizontal cut of the ambiguity function) for a moving target, with the true location always being located in between the two peaks, allowing for correct range detection.

The suggested CS process can serve to retain a lot of the advantages of the desired waveform, while also making sure it is hard to spoof by artificial Doppler modulation. In fact, the result is well known for the special case of FMCW radars, which implement the matched filter in hardware by mixing the received signal with the transmitted chirp, as will be done in the experiment ahead. To detect the Doppler shift of the target, a triangular frequency modulation can be used with an up chirp followed by a down chirp, producing two peaks in the spectrum of the mixer's output, with the distance between the peaks proportional to the velocity of the target, and its location proportional to the mean of the peaks. The CS process suggested here expands this result to all Doppler-tolerant waveforms.

IV. Experimental Verification–Range Deception of FMCW Radars

To support the formulation described in Section II, an experiment was conducted in the anechoic chamber as shown in Fig. 3. An FMCW radar was constructed by up-converting a 40 MHz linear down-chirp with a period of 50 μs, produced by an AFG-3051, to the central frequency of 750 MHz. The radar used a circulator for isolation of the transmitting and receiving channels, which were both fed by the same UHF

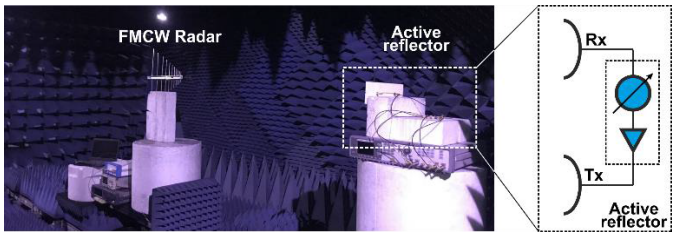

Fig. 3. Experimental set up in the anechoic chamber, an FMCW radar is directed at a time-modulated scatterer. The schematic inset shows the electronics of the scatterer, allowing fully dynamic reflected phase control.

log-periodic antenna (CLP5130-2, 105–1300 MHz). The time-modulated scatterer that is shown in Fig. 3 was assembled from a pair of identical dipole antennas (W1096), which were connected with a long delay line made out of cables to simulate a more distant target (cables introduce an additional delay, while the entire system mimics a point-like scatterer). A phase shifter (AD8340) was placed along the connecting line as seen in the inset to Fig. 3. This time-modulated scatterer represents the analog of a single meta-atom which could be placed in an array that forms a time-dependent metasurface. In this configuration, the additional phase on the signal, guided between Rx and Tx antennas mimics the reflection phase, imprinted by a point scatterer. As the instantaneous frequency is the time-derivative of phase, linear temporal modulation of the latter leads to the conventional Doppler shift.

The phase shifter was dynamically controlled by a biasing voltage applied to a vector modulator (AD8340), capable of providing an arbitrary time-dependent phase profile. An amplifying stage was added following the phase shifter in order to compensate for the losses in the cables, yet it is not necessary for the experiment. Typically, 20 dB can be added in the case of low-intensity input signals, not saturating the amplifier. It is also important to stress that the power reaching the amplifier is too low to cause intermodulation distortion effects. The reflected signal from the time-modulated scatterer was picked up by the radar's antenna and was continuously mixed with the transmitted chirp to produce the baseband output. The baseband was low pass filtered before being observed in the frequency domain using a sampling scope, as can be seen on the insets in Fig. 4. The signal at the baseband can be computed by using (3) and solving

$$s_{\text{baseband}}(t) = \text{Re}\{s_{\text{LFM}}(t)\}\text{Re}\{s_{\text{LFM}}(t-\tau)e^{-i\omega_D t}\} \approx \text{Cos}\left(\underbrace{\left(\frac{\Delta_\omega \tau}{T}+\omega_D\right)}_{\omega_{\text{baseband}}} t\right) u\left(\frac{t-\tau}{T-\tau}\right) \quad (7)$$

where we have neglected the second harmonic of the carrier, which is outside of the bandwidth of the filter, as well as the phases and contributions of the mixing between the reflected echo with the next transmitted chirp (assuming $T \gg \tau$). The use of the real operator is required before multiplication in (7) seeing as mixing is a non-linear operation. The resulting dominant frequency at the baseband ω_{baseband} is therefore a function of the delay and Doppler, and its measurement allows

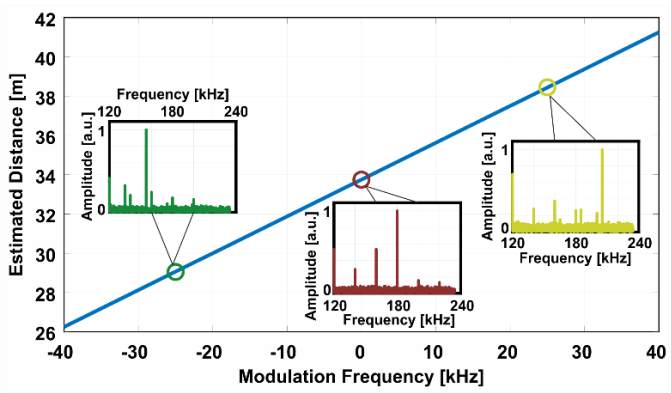

Fig. 4. Demonstration of full control over the perceived range of the static time-modulated scatterer. By controlling the modulation frequency of the reflected phase from the object, it may appear further and even closer than it truly is. Insets show the baseband signal at the FMCW radar for selected modulation frequencies.

calculating the range of the target

$$R = \frac{cT}{2|\Delta_\omega|}(\omega_{\text{baseband}} - \text{sign}(\Delta_\omega)\omega_D) \quad (8)$$

where $\text{sign}(x) = \begin{cases} +1 x > 0 \\ -1 x < 0 \end{cases}$ and we assumed without loss of generality that $|(\Delta_\omega \tau/T)| < |\omega_D|$. (8) clearly reveals the coupling between range and Doppler that was explored in the theoretical section through the prism of the ambiguity function, where positive Doppler shifts (approaching targets) represent up-conversion of the reflected chirp, and negative shifts (receding targets) represent down conversion of the chirp.

The phase shifter of the time-modulated scatterer was configured to imprint fake Doppler signatures, on the reflected echoes, while the corresponding distance of the target was deduced from measuring the dominant frequency at the baseband of the radar receiver (see insets to Fig. 4) and using (8) with $\omega_D = 0$. The results are plotted in Fig. 4, where a linear relation can be observed between the modulation frequency, which corresponds to the fake Doppler shift frequency, and the estimated range of the target. This linear relationship is in very good agreement with the results derived in (8) and Fig. 2, demonstrating full control over the perceived location of the target, and even making it possible to create the illusion that the target is closer than it really is.

The insets in Fig. 4 show the baseband signals recorded by the sampling scope (MFLI Lock-in Amplifier, which can achieve a sampling rate of up to 60 MSa/s) at each of the corresponding modulation frequencies. Some additional peaks can be observed and they are attributed in small part to multipath interference and the neglection of some terms in the derivation leading to (7). The most prominent source however is the formation of the so-called "picket fence" that arises whenever a periodic signal is sampled, forming an equidistant comb around the dominant peak, sometimes even obscuring it. The root cause is related to the periodicity of the phase modulation and the continuously transmitted radar waveforms.

A final noteworthy comment concerns an additional way to countermeasure such range deception in the special case

of FMCW waveforms, as revealed by the expression for the baseband frequency ω_{baseband} in (7). By alternating the chirp rate T, it is possible to deduce the Doppler shift (whether due to real motion or by time-dependent phase modulation) ω_D, which also achieves successful decoupling of range and Doppler measurements. While this result strictly applies only to the case of FMCW, it can be expected to work for other waveforms as well (albeit with different calculation methods suitable for the specific signal of choice). This adds another parameter of diversity that can serve a useful purpose, much like alternating PRF is commonly used today to resolve range and Doppler ambiguity.

V. Outlook and Conclusion

A temporal phase modulation approach for radar deception was demonstrated. In contrast with existing passive (e.g., stealth and metamaterials) and active (e.g., jamming, spoofing) approaches, the time-modulation of the reflected echoes requires neither complex shaping of enclosures around a target nor expensive and cumbersome power-consuming electronics. Here, we introduced a deception concept, which is based on traversing "journeys" along the ambiguity function, which characterizes the radar's measurement accuracy, taking advantage of the signal processing weaknesses that are inherent to a very broad class of radar systems. We have demonstrated that Doppler-tolerant waveforms are susceptible to range deception by exploiting one of their greatest strengths, but also provided a solution to counter these shortcomings with a simple process of conjugately symmetrizing the transmitted waveforms. In particular, we showed experimentally that FMCW radars can interpret targets with time-modulated scattering cross-sections as if they were closer than they truly are. While this behavior might at first glance contradict the laws of relativity, a reasonable objection had the target been interrogated by a short pulse, this is shown to be perfectly normal in the context of Doppler tolerant waveforms that rely on matched filters, paving the way for temporal-phase deception strategies. As an outlook, the proposed concept can be used to conceal large targets. In this case, time-modulated metasurfaces, capable of providing dynamic 2π control over the phase, can be used to cover scattering centers of interest. Another application concerns smart electromagnetic chaff, which can be used for creating fake radar targets that correctly mimic the expected Doppler velocity. While classical "static chaff" is straightforwardly filtered out with clutter filters, smart time-modulated structures are immune against those countermeasures.

References

[1] R. Klemm, H. Griffiths, and W. Koch, *Novel Radar Techniques and Applications*, vol. 2. Institution of Engineering and Technology, 2017.

[2] M. Mahfouz, A. Fathy, Y. Yang, E. E. H. Ali, and A. Badawi, "See-through-wall imaging using ultra wideband pulse systems," in *Proc. 34th Appl. Imag. Pattern Recognit. Workshop (AIPR)*, 2005, pp. 48–53.

[3] J. S. Lee, C. Nguyen, and T. Scullion, "A novel, compact, low-cost, impulse ground-penetrating radar for nondestructive evaluation of pavements," *IEEE Trans. Instrum. Meas.*, vol. 53, no. 6, pp. 1502–1509, Dec. 2004.

[4] M. Murad, J. Nickolaou, G. Raz, J. S. Colburn, and K. Geary, "Next generation short range radar (SRR) for automotive applications," in *Proc. IEEE Radar Conf.*, May 2012, pp. 214–219.

[5] P. Van Dorp and F. C. A. Groen, "Human walking estimation with radar," *IEE Proc., Radar Sonar Navigat.*, vol. 150, no. 5, pp. 356–365, 2003.

[6] C. Gu, C. Li, J. Lin, J. Long, J. Huangfu, and L. Ran, "Instrument-based noncontact Doppler radar vital sign detection system using heterodyne digital quadrature demodulation architecture," *IEEE Trans. Instrum. Meas.*, vol. 59, no. 6, pp. 1580–1588, Jun. 2010.

[7] V. Kozlov, D. Vovchuk, S. Kosulnikov, D. Filonov, and P. Ginzburg, "Micro-Doppler signatures of subwavelength nonrigid bodies in motion," *Phys. Rev. B, Condens. Matter*, vol. 104, no. 5, pp. 1–6, 2021.

[8] R. Komissarov, V. Kozlov, D. Filonov, and P. Ginzburg, "Partially coherent radar unties range resolution from bandwidth limitations," *Nature Commun.*, vol. 10, no. 1, pp. 1–9, Mar. 2019.

[9] D. Kissinger, *Millimeter-Wave Receiver Concepts for 77 GHz Automotive Radar in Silicon-Germanium Technology*. New York, NY, USA: Springer, 2012.

[10] R. Zetik, J. Sachs, and R. Thoma, "UWB short-range radar sensing—The architecture of a baseband, pseudo-noise UWB radar sensor," *IEEE Instrum. Meas. Mag.*, vol. 10, no. 2, pp. 39–45, Apr. 2007.

[11] S. Feng, N. Mughees, and V. Wollesen, "Reviewing the application and integration of software defined radios to radar systems," in *Proc. IEEE Radar Conf. (RadarConf)*, Sep. 2020, pp. 1–6.

[12] H. Zhang, L. Li, and K. Wu, "24 GHz software-defined radar system for automotive applications," in *Proc. 10th Eur. Conf. Wireless Technol.*, Oct. 2007, pp. 138–141.

[13] P. M. Grant and J. H. Collins, "Introduction to electronic warfare," *IEE Proc. F, Commun. Radar Signal Process.*, vol. 129, no. 3, pp. 113–132, Jun. 1982.

[14] L. Neng-Jing and Z. Yi-Ting, "A survey of radar ECM and ECCM," *IEEE Trans. Aerosp. Electron. Syst.*, vol. 31, no. 3, pp. 1110–1120, Jul. 1995.

[15] F. A. Butt, I. H. Naqvi, and A. I. Najam, "Radar ECCM against deception jamming: A novel approach using bi-static and mono-static radars," in *Proc. 15th Int. Multitopic Conf. (INMIC)*, Dec. 2012, pp. 137–141.

[16] D. J. Bachmann, R. J. Evans, and B. Moran, "Game theoretic analysis of adaptive radar jamming," *IEEE Trans. Aerosp. Electron. Syst.*, vol. 47, no. 2, pp. 1081–1100, Apr. 2011.

[17] G. Frazer, A. Balleri, and G. Jacob, "Deception jamming against Doppler beam sharpening radars," *IEEE Access*, vol. 8, pp. 32792–32801, 2020.

[18] R. Chauhan, "A platform for false data injection in frequency modulated continuous wave radar," Utah State Univ., Logan, UT, USA, 2014.

[19] G. A. Rao and S. P. Mahulikar, "Integrated review of stealth technology and its role in airpower," *Aeronaut. J.*, vol. 106, no. 1066, pp. 629–642, Dec. 2002.

[20] W. F. Bahret, "The beginnings of stealth technology," *IEEE Trans. Aerosp. Electron. Syst.*, vol. AES-29, no. 4, pp. 1377–1385, Oct. 1970.

[21] C. Chi-Hao and J. Tsui, *An Introduction to Electronic Warfare; From the First Jamming to Machine Learning Techniques*. Denmark: River Publisher, 2021.

[22] S. Kosulnikov et al., "Circular wire-bundle superscatterer," *J. Quant. Spectrosc. Radiat. Transf.*, vol. 279, Mar. 2022, Art. no. 108065.

[23] D. Dobrykh et al., "Multipole engineering for enhanced backscattering modulation," *Phys. Rev. B, Condens. Matter*, vol. 102, no. 19, Nov. 2020, Art. no. 195129.

[24] D. Filonov, A. Shmidt, A. Boag, and P. Ginzburg, "Artificial localized magnon resonances in subwavelength meta-particles," *Appl. Phys. Lett.*, vol. 113, no. 12, Sep. 2018, Art. no. 123505.

[25] R. Komissarov and A. Wool, "Spoofing attacks against vehicular FMCW radar," in *Proc. 5th Workshop Attacks Solutions Hardw. Secur.*, Nov. 2021, pp. 91–97.

[26] A. Lazaro, A. Porcel, M. Lazaro, R. Villarino, and D. Girbau, "Spoofing attacks on FMCW radars with low-cost backscatter tags," *Sensors*, vol. 22, no. 6, p. 2145, Mar. 2022.

[27] D. Feng, L. Xu, X. Pan, and X. Wang, "Jamming wideband radar using interrupted-sampling repeater," *IEEE Trans. Aerosp. Electron. Syst.*, vol. 53, no. 3, pp. 1341–1354, Jun. 2017.

[28] D. H. A. Maithripala and S. Jayasuriya, "Radar deception through phantom track generation," in *Proc., Amer. Control Conf.*, 2005, pp. 4102–4106.

[29] J. Zhang, D. Zhu, and G. Zhang, "New antivelocity deception jamming technique using pulses with adaptive initial phases," *IEEE Trans. Aerosp. Electron. Syst.*, vol. 49, no. 2, pp. 1290–1300, Apr. 2013.

[30] Z. Liu, J. Sui, Z. Wei, and X. Li, "A sparse-driven anti-velocity deception jamming strategy based on pulse-doppler radar with random pulse initial phases," *Sensors*, vol. 18, no. 4, pp. 1–17, 2018.

[31] C. Zhou, Z.-B. Zhu, and Z.-Y. Tang, "A novel waveform design method for shift-frequency jamming confirmation," *Int. J. Antennas Propag.*, vol. 2018, no. 2, pp. 1–13, Jul. 2018.

[32] F. Capolino, *Applications of Metamaterials*. Boca Raton, FL, USA: CRC Press, 2017.
[33] N. Engheta and R. W. Ziolkowski, *Electromagnetic Metamaterials: Physics and Engineering Explorations*, 1st ed. Hoboken, NJ, USA: Wiley, 2006.
[34] D. R. Smith, J. B. Pendry, and M. C. K. Wiltshire, "Metamaterials and negative refractive index," *Science*, vol. 305, no. 5685, pp. 788–792, 2004.
[35] D. Schurig et al., "Metamaterial electromagnetic cloak at microwave frequencies," *Science*, vol. 314, no. 5801, pp. 977–980, Nov. 2006.
[36] P. Alitalo and S. Tretyakov, "Electromagnetic cloaking with metamaterials," *Mater. Today*, vol. 12, no. 3, pp. 22–29, Mar. 2009.
[37] R. Fleury and A. Alu, "Cloaking and invisibility: A review," *Prog. Electromagn. Res.*, vol. 147, pp. 171–202, 2014.
[38] V. Kozlov, D. Vovchuk, and P. Ginzburg, "Broadband radar invisibility with time-dependent metasurfaces," *Sci. Rep.*, vol. 11, no. 1, pp. 1–11, Jul. 2021.
[39] X. G. Zhang et al., "Smart Doppler cloak operating in broad band and full polarizations," *Adv. Mater.*, vol. 33, no. 17, 2021, Art. no. 2007966.
[40] B. Liu, Y. He, S.-W. Wong, and Y. Li, "Experimental demonstration of a time-domain digital-coding metasurface for a Doppler cloak," *Opt. Exp.*, vol. 29, no. 2, p. 740, 2021.
[41] B. Liu, H. Giddens, Y. Li, Y. He, S.-W. Wong, and Y. Hao, "Design and experimental demonstration of Doppler cloak from spatiotemporally modulated metamaterials based on rotational Doppler effect," *Opt. Exp.*, vol. 28, no. 3, p. 3745, 2020.
[42] D. Ramaccia, D. Sounas, A. Alu, A. Toscano, and F. Bilotti, "Phase-induced frequency conversion and Doppler effect with time-modulated metasurfaces," *IEEE Trans. Antennas Propag.*, vol. 68, no. 3, pp. 1607–1617, Mar. 2020.
[43] M. Liu, A. B. Kozyrev, and I. V. Shadrivov, "Time-varying metasurfaces for broadband spectral camouflage," *Phys. Rev. Appl.*, vol. 12, no. 5, Nov. 2019, Art. no. 054052.
[44] X. Wang and C. Caloz, "Spread-spectrum selective camouflaging based on time-modulated metasurface," *IEEE Trans. Antennas Propag.*, vol. 69, no. 1, pp. 286–295, Jan. 2021.
[45] N. Levanon and E. Mozeson, *Radar Signals*. Hoboken, NJ, USA: Wiley, 2004.
[46] M. A. Richards, J. Scheer, and W. Holm, *Principle of Modern Radar*. Rijeka, Croatia: SciTech, 2010.
[47] M. I. Skolnik, *Radar Handbook*. New York, NY, USA: McGraw-Hill, 2008.
[48] P. Setlur, J. Hollon, K. T. Arasu, and M. Rangaswamy, "On a formal measure of Doppler Tolerance," in *Proc. IEEE Radar Conf. (RadarConf)*, May 2017, pp. 1751–1756.
[49] A. W. Rihaczek, "Doppler-tolerant signal waveforms," *Proc. IEEE*, vol. 54, no. 6, pp. 849–857, Jun. 1966.
[50] S. H. S. Baher, "A review of radar signals in terms of Doppler tolerance, time-sidelobe level, and immunity against jamming," *Int. J. Microw. Wireless Technol.*, vol. 10, no.10, pp. 1134–1142, Dec. 2018.
[51] W. Jia, Y. Cao, S. Zhang, and W.-Q. Wang, "Detecting high-speed maneuvering targets by exploiting range-Doppler relationship for LFM radar," *IEEE Trans. Veh. Technol.*, vol. 70, no. 3, pp. 2209–2218, Mar. 2021.
[52] L. Bruno, P. Braca, J. Horstmann, and M. Vespe, "Experimental evaluation of the range–Doppler coupling on HF surface wave radars," *IEEE Geosci. Remote Sens. Lett.*, vol. 10, no. 4, pp. 850–854, Jul. 2013.

Vitali Kozlov received the B.Sc. degree in physics, the B.Sc. degree in electrical and electronics engineering, and the M.Sc. degree from Tel Aviv University, Tel Aviv, Israel, in 2015, 2015, and 2017, respectively, where he is currently pursuing the Ph.D. degree.

His research interests include time-dependent scattering phenomena, dynamic metasurfaces, and their application toward radar and communication.

Dmytro Vovchuk received the B.Sc. and M.Sc. degrees from Yuriy Fedkovych Chernivtsi National University, Chernivtsi, Ukraine, in 2012 and 2013, respectively.

He has been performing his research with the School of Electrical Engineering, Tel Aviv University, Tel Aviv, Israel, since 2019. His research interests include radars, superscattering and superdirectivity, micro-Doppler, and deterministic chaos for communication systems.

Pavel Ginzburg (Member, IEEE) received the Ph.D. degree from Technion, Haifa, Israel, in 2011.

He is currently an Associate Professor with Tel Aviv University, Tel Aviv, Israel. He is also a former EPSRC Research Fellow, an International Newton Research Fellow, and a Rothschild Fellow with the King's College London, London, U.K. He is also the Head of the "Dynamics of Nanostructures" Laboratory, encompassing theoretical group, optical spectroscopy, and radio waves labs. The laboratory runs multidisciplinary research in the field of bio-photonics, quantum mechanics, nano-plasmonics and metamaterials, and radio physics.